2021 American Control Conference (ACC)
New Orleans, USA, May 25-28, 2021

Towards State-of-Charge Estimation for Battery Packs: Reducing Computational Complexity by Optimising Model Sampling Time and Update Frequency of the Extended Kalman Filter

F.S.J. Hoekstra H.J. Bergveld M.C.F. Donkers

Abstract— **Accurate State-of-Charge (SoC) estimation remains a challenge for large battery packs. This paper aims to reduce the computational complexity of single-cell estimation, which already achieves satisfactory performance, such that it can be more easily scaled to large arrays of cells inside battery packs. This is done by experimenting with a range of sampling times for the models used in an Extended Kalman Filter (EKF) and by adjusting the update frequency of this estimator. The EKF is tested with linear time-invariant and linear parameter-varying models and also in joint state-parameter estimation form. Results show that adjusting the sampling time and update frequency can result in a significant reduction of computational complexity, around a factor of 148, while only suffering a minor increase in SoC estimation error. This means that a relatively small micro-controller can be employed to estimate the SoC of an entire battery pack.**

I. Introduction

Over the past 20 years, research related to estimation for Li-ion batteries has mainly focused on State-of-Charge (SoC) estimation [1]. Although the SoC is often not directly displayed to the user, it is a key parameter in determining, e.g., the range of an electric vehicle. In search for the best SoC estimation algorithm, a vast amount of research has led to numerous different solutions. These range from basic approaches such as Coulomb counting [2], to more advanced methods which use machine learning, see, e.g., [3]. The most popular approach, however, is the model-based estimation problem, as first introduced in [4], and later expanded by many others, see, e.g., [4]–[7] and references therein.

Model-based methods aim to match the prediction of a battery model with the measured reality, by adjusting one or more states and/or parameters of the model. The trade-off between model predictions and measurements is made by an observer or estimator, of which there exists a variety of options, as reviewed in [1, 5]. Most popularly, the Extended Kalman Filter (EKF) is used as estimator, see, e.g., [6], for its ability to deal with nonlinear models which are often used for batteries. Although there are a number of variations on the Kalman Filter (KF), as found in, e.g., [1, 5], they typically bring marginal improvement to the estimates while coming at increased computational complexity [7], when compared to the EKF. Instead, one should keep in mind that battery packs can consists of thousands of cells and thus manageable computational complexity is a top priority for battery-pack SoC estimation algorithms.

Therefore, literature rightfully focuses on reducing the computational complexity associated with SoC estimation for a large number of cells, see, e.g., [8]–[10]. For instance in [9], states and parameters of all cells are estimated, based on one lumped cell and the differences between cells are compared to this 'meta-cell'. In [8], four different options are compared, ranging from treating the pack as a single lumped cell to only estimating the SoC of the fullest and most empty cell. The drawback is that these approaches make certain simplifications, thus most likely harming the SoC estimation accuracy. Instead, one can also aim to reduce the computational demand of single-cell SoC estimation, thus allowing it to scale to a full-sized pack. To the authors' knowledge, an unexplored option is to examine the effect of the update frequency and sampling time of the model of the EKF on its performance.

In this paper, the trade-off between the SoC estimation accuracy and computation time of the EKF with respect to its update frequency is investigated. This is done by 1) experimenting with the sampling time and the type of model used in the EKF, and 2) varying the frequency with which the EKF is updated. The empirical models are all first-order electrical models, but one has constant parameters, i.e., Linear Time-Invariant (LTI) and two have SoC-dependent parameters in the form of Linear Parameter-Varying (LPV) models. In total four forms of the EKF are evaluated, three with the aforementioned models and one Joint EKF (JEKF). As estimator, we apply the EKF with forgetting factor presented in [11], whose one-knob tuning simplifies the comparison between the four forms of the EKF. This allows us to easily investigate the use of prediction and update steps at different frequencies. The models are fitted on one dynamic data set and the SoC estimation performance is validated on four other sets of dynamic data.

II. Modelling

The battery terminal voltage and internal state behaviour can be modelled using a discrete-time nonlinear model, as given by

$$\begin{cases} \begin{bmatrix} s_{k+1} \\ o_{k+1} \end{bmatrix} = \begin{bmatrix} 1 & 0 \\ 0 & \theta^1(s_k) \end{bmatrix} \begin{bmatrix} s_k \\ o_k \end{bmatrix} + \begin{bmatrix} \frac{T_s}{C_0} \\ \theta^2(s_k) \end{bmatrix} u_k, \\ y_k = V^{\text{emf}}(s_k) + o_k + \theta^3(s_k) u_k, \end{cases} \quad (1)$$

The authors are with the Dept. of Electrical Engineering, Eindhoven University of Technology, Netherlands. Henk Jan Bergveld is also with NXP semiconductors, Eindhoven, Netherlands. Email: {f.s.j.hoekstra,h.j.bergveld,m.c.f.donkers}@tue.nl.

This project receives funding from the European Union's Horizon 2020 research and innovation programme under Grant Agreement no. 957273.

Authorized licensed use limited to: Technische Hochschule Deggendorf. Downloaded on September 13,2024 at 20:15:36 UTC from IEEE Xplore. Restrictions apply.

where s_k is the SoC, which satisfies $0 \leq s_k \leq 1$, o_k the dynamic part of the overpotential, y_k the terminal voltage and u_k is the current input, with k the time index. Furthermore, T_s is the sampling time, C_0 the cell capacity, $V^{\text{emf}}(s_k)$ the Electro-motive Force (EMF), also know as the open-circuit voltage, $\theta^1(s_k)$, $\theta^2(s_k)$, $\theta^3(s_k)$ are SoC-dependent parameters that capture the overpotential dynamics.

Current and voltage are continuous signals, i.e. $u(t)$ and $y(t)$, respectively, with $t \in \mathbb{R}$, but in any practical BMS, they will only be available at discrete time instances. We assume in this paper that currents and voltages are sampled at a measurement sample time T_m, leading to a sequence of current and voltage measurements given by $\{u(0), u(T_m), u(2T_m), \ldots, u((L-1)T_m)\}$ and $\{y(0), y(T_m), y(2T_m), \ldots, y((L-1)T_m)\}$, with L the available number of measurements. Even though these measurements are available every T_m seconds, the model (1) can be calculated at a larger sampling interval $T_s = MT_m$, with downsampling factor $M \in \mathbb{N}$, leading to a reduction in the amount of data that needs to be processed by the BMS. This means that the model (1) only uses current inputs $u_k = u(kT_s) = u(kMT_m)$ and produces voltages $y(kT_s) = y(kMT_m)$. We only use data with sample time $T_m = 1s$ and therefore we choose to keep $T_s = M$ throughout this study. In this paper, we will explore this idea of downsampling to achieve a computational reduction of estimating the SoC, possibly leading to a (small) decrease in SoC estimation accuracy. The remainder of this section will briefly discuss the EMF after which the identification of the overpotential dynamics will be explained in detail.

A. Electromotive-Force

In order to correctly identify the overpotential dynamics, one should first separate the nonlinear offset, i.e., the EMF, from the terminal voltage. The data used in this paper has previously been used in [11] and has been measured on a $12.5Ah$ Lithium Nickel Cobalt Aluminium Oxide (LiCoNAlO2) cell. The EMF-SoC relation is obtained using a pulse-discharge experiment which starts with SoC intervals of 5% and is followed by shorter pulses when the lower voltage limit is reached for the first time. The slope of the EMF is gradual, i.e., no plateaus, over the SoC range which is inherent to the cell chemistry.

B. Overpotential model

Having obtained the EMF, we first separate the overpotential behaviour from the overall battery behaviour, i.e., the EMF is subtracted from the terminal voltage, as given by

$$y_k^o = y(t) - V^{\text{emf}}(s_k), \tag{2}$$

where y_k^o is the overpotential. This behaviour can locally, i.e., at a certain SoC or temperature, be captured by an LTI model, but nonlinear behaviour occurs when considering the entire operating range. In order to accurately model this, an LPV model can be used. In general, there are two approaches to identify an LPV model, the local and the global approach [12]. In the first method, the battery is excited at multiple operating points and LTI models are identified for each of these regions, see, e.g., [13]. The general conception is that the local approach requires multiple isolated experiments, e.g., pulses at specific SoC points. Instead, we divide a single dynamic data set into smaller sections, thus fitting models on each of these intervals. This allows the local approach to be used on data that is recorded during regular operation of the battery pack.

For all models we consider a first-order Auto-Regressive with eXogenous inputs (ARX) model, where a local instance of this model is given by

$$\hat{y}_k^o = -a_1^i y_{k-1}^o + b_0^i u_k + b_1^i u_{k-1}, \tag{3}$$

where $\hat{y}_k^o$ is the output prediction and a_1^i, b_0^i and b_1^i are the model parameters estimated by solving the convex least-squares minimisation problem

$$\min_{a_1^i, b_0^i, b_1^i} \quad \sum_{k \in \mathcal{K}^i} \|y_k^o - \hat{y}_k^o\|_2^2, \tag{4}$$

subject to (3), where $\mathcal{K}^i = \{K^{i-1}, \ldots, K^i - 1\}$ is a certain interval of the data with $K^{i-1} < K^i$, $K^0 = 0$, $K^I = \left\lceil \frac{L}{M} \right\rceil$ where $\left\lceil \frac{L}{M} \right\rceil$ is the number of available measurements used during modelling and where $\lceil\ \rceil$ denotes rounding upwards to the next integer. Furthermore, $i \in \mathcal{I} = \{1, \ldots, I\}$ is the interval number with I the total number of intervals, the selection of which will be discussed in Section IV. Note that $I = 1$ yields an LTI model and is thus omitted from the interval options. In order to obtain the SoC-dependent parameters of (1), each set of parameters $\{a_1^i,\ b_0^i,\ b_1^i\}$ is assigned to the average SoC of that interval, given by

$$\overline{s}^i = \tfrac{1}{n(\mathcal{K}^i)} \sum_{k \in \mathcal{K}^i} s_k, \tag{5}$$

where $n(\mathcal{K}^i)$ is the number of elements in or cardinality of set $\mathcal{K}^i$. The overall nonlinear behaviour is now captured by

$$\begin{aligned} \theta^1(s) &= \{-a_1^1, \ldots, -a_1^I\}, \\ \theta^2(s) &= \{(b_1^1 - a_1^1 b_0^1), \ldots, (b_1^I - a_1^I b_0^I)\}, \\ \theta^3(s) &= \{b_0^1, \ldots, b_0^I\}, \end{aligned} \tag{6}$$

where values in between the scheduling points are found by linearly interpolating between the local LTI models with respect to the scheduling variable. This model comes down to creating a look-up table for the dynamic parameters, as is commonly done for modelling batteries, see, e.g., [14]. In the remainder of this paper, we will refer to models obtained via the local approach with the abbreviation L-LPV.

For the global approach one data set is typically used in which the scheduling variable changes dynamically and a certain functional dependency of the parameters with respect to the scheduling variable is identified, see, e.g., [15]. However, the functional dependency is often unknown upfront, so one would either try to find the correct basis function or settle on a sub-optimal one. A way to determine the correct basis function is to use the local approach, as the collection of LTI models can provide an indication of the type of required functional dependency.

Authorized licensed use limited to: Technische Hochschule Deggendorf. Downloaded on September 13,2024 at 20:15:36 UTC from IEEE Xplore. Restrictions apply.

Taking this reasoning one step further, one can directly estimate the functional dependency on the local models, thus not using the input-output data as done in problem (4), which for the global approach requires solving a nonlinear optimisation problem. The problem at hand is then given by

$$\min_{p} \quad \sum_{i\in\mathcal{I}} \left\|\theta(\overline{s}^i) - \Theta(p,\overline{s}^i)\right\|_2^2, \tag{7}$$

where $\Theta(p,s)$ is an SoC-dependent function and p is the set of parameters used in Θ. The exact functional dependency used in this paper will be provided in Section IV. Models with this functional dependency of the parameters will be referred to as F-LPV.

The benefit of using a functional dependency of the parameters is that it may be faster in terms of implementation, since there is no need for interpolation as one would require for a model acquired through the local approach. On the other hand, the look-up table can take any form, thus allowing more freedom in the dependencies which can result in more precise models. The overall predictive quality of both approaches will be discussed in Section IV.

III. Extended Kalman Filter

The algorithm used for SoC estimation in this paper is the EKF with cross-correlation and forgetting factor proposed in [11], which allows one-knob tuning, instead of standard noise-variance tuning. The EKF is used because it is considered to be a good all-rounder [16]. The EKF is given by

$$\begin{aligned}
P_{k+1}^{-} &= (F_k - S_k R_k^{-1} H_k) P_k (F_k - S_k R_k^{-1} H_k)^\top + Q_k \\
&\quad - S_k R_k^{-1} S_k^\top && \text{(8a)}\\
\hat{x}_{k+1}^{-} &= A_k \hat{x}_k + B_k u_k + S_k R_k^{-1}(y(t) - \hat{y}_k) && \text{(8b)}\\
K_k &= P_{k+1} H_k^\top (H_k P_{k+1} H_k^\top + \gamma R_k)^{-1} && \text{(8c)}\\
P_{k+1}^{+} &= \tfrac{1}{\gamma}(I - K_k H_k) P_{k+1} && \text{(8d)}\\
\hat{x}_{k+1}^{+} &= \hat{x}_{k+1} + K_k(y(t) - \hat{y}_k) && \text{(8e)}
\end{aligned}$$

where $S_k = 0$ provides a standard EKF and $\gamma < 1$ is the forgetting factor which is the only tuning parameter.

In this study, four variations of the ARX overpotential model are used: LTI, L-LPV, F-LPV, and with adaptive parameters, i.e., a Joint EKF, as also used in [11]. For each of these, the size and content of the parameters in (8) are different. The first three models all share the same state $x_k = \begin{bmatrix} s_k & o_k \end{bmatrix}^\top$ and corresponding to this we have

$$Q_k = \begin{bmatrix} \frac{T_s^2}{C_0^2} & \frac{T_s \theta_k^2}{C_0} \\ \frac{T_s \theta_k^2}{C_0} & (\theta_k^2)^2 \end{bmatrix},\ S_k = \begin{bmatrix} \frac{\theta_k^3}{C_0} \\ \theta_k^2 \theta_k^3 \end{bmatrix},\ R_k = (1+\theta_k^3)^2, \tag{9}$$

for details see [11]. For the LTI model, we have

$$\begin{aligned}
A = F &= \begin{bmatrix} 1 & 0 \\ 0 & \theta^1 \end{bmatrix}, \\
B &= \begin{bmatrix} \frac{T_s}{C_0} & \theta^2 \end{bmatrix}^\top,\ H_k = \begin{bmatrix} \nabla V^{\mathrm{emf}}(s_k) & 1 \end{bmatrix},
\end{aligned} \tag{10}$$

in which ∇ denotes the numerical gradient, i.e., $\nabla V^{\mathrm{emf}}(s_k) = \frac{V^{\mathrm{emf}}(s_k+\epsilon) - V^{\mathrm{emf}}(s_k-\epsilon)}{2\epsilon}$, where ϵ is a minor deviation in s, and where A, F and B are constant while H_k is time-dependent. Note that since θ^1, θ^2, θ^3 are constants here, we also have constant Q, S and R for the LTI model. Second, for the L-LPV and F-LPV models we have

$$\begin{aligned}
A_k &= \begin{bmatrix} 1 & 0 \\ 0 & \theta^1(s_k) \end{bmatrix}, B_k = \begin{bmatrix} \frac{T_s}{C_0} & \theta^2(s_k) \end{bmatrix}^\top, \\
F_k &= \begin{bmatrix} 1 & 0 \\ \nabla\theta^1(s_k) o_k + \nabla\theta^2(s_k) u_k & \theta^1(s_k) \end{bmatrix}, \\
H_k &= \begin{bmatrix} \nabla V^{\mathrm{emf}}(s_k) + \nabla\theta^3(s_k) u_k & 1 \end{bmatrix},
\end{aligned} \tag{11}$$

where $\theta(s)$ can be replaced with $\Theta(p,s)$ to obtain the EKF matrices for the F-LPV model. This also allows us to use the analytical gradient for the EKF parameters instead of the numerical gradient. Finally, for the JEKF the state vector is first extended, as given by

$$x_k = \begin{bmatrix} s_k & o_k & \theta_k^1 & \theta_k^2 & \theta_k^3 \end{bmatrix}^\top, \tag{12}$$

such that the overpotential parameters are estimated online. The corresponding Q, S, R, A, B, F and H can be found in [11]. With the four variations of the EKF explained, we will present the exact modelling procedure and discuss the obtained model accuracy.

IV. Modelling Results

In this section, we identify the LTI, L-LPV and F-LPV models from Section II. Each of these models will be identified separately for a range of combinations of sampling times $T_s \in \{1, 2, \ldots, 50\}s$ and intervals $I \in \{2, 3, \ldots, 50\}$. First, we will consider the data, which is available at times $T_m = 1s$, on which the models are identified and we will provide an example of the L-LPV and F-LPV models. After this, the model performance is shown for the identification data and subsequently tested for the validation data. Lastly, we consider the effect of averaging current measurements available at a higher frequency than that of the model, thus downsampling the inputs without omitting intermediary data.

A. Identification data and functional dependencies

Dynamic current cycles have been drawn from the same cell from which the EMF was extracted [11]. One of these cycles is shown in Fig. 1, and is used to identify all the models. It features a predominantly discharge-oriented profile which continues until the lower voltage limit is violated. For the local approach, this data set is divided into I intervals, the selection of which is a trade-off between the accuracy with which certain dynamics are coupled to the correct corresponding scheduling variable SoC and the number of data points available for solving the local problem (4). In terms of selection of the intervals, we choose to split the data in pieces of equal length, thus maximising the amount of data points underlying each local model. Alternatively, one could construct the intervals based on differences in SoC. However, as the sampling time increases, and fewer data points are thus included in the estimation problem, poor local models can occur due to insufficient data points.

Authorized licensed use limited to: Technische Hochschule Deggendorf. Downloaded on September 13,2024 at 20:15:36 UTC from IEEE Xplore. Restrictions apply.

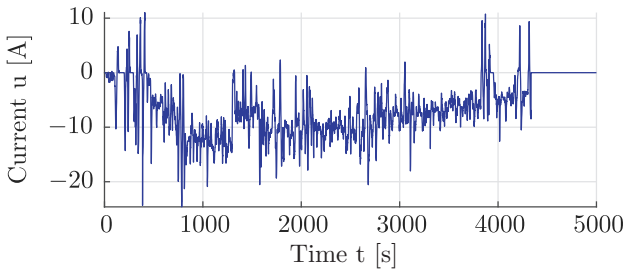

(a) Current

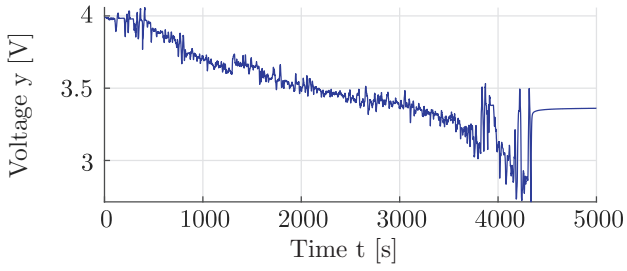

(b) Voltage

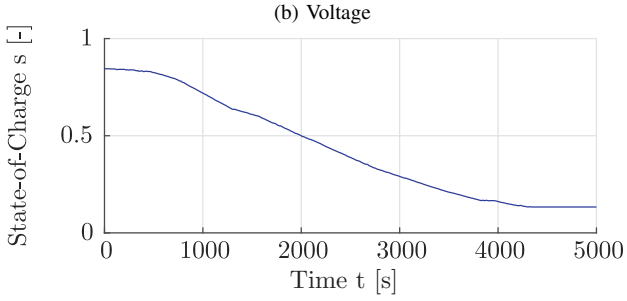

(c) State-of-Charge

Fig. 1: Overview of the identification data, with $T_m = 1s$.

To clarify the functional dependencies used in the F-LPV model, we consider the example where the sampling time $T_s = T_m = 1s$ and the number of intervals $I = 25$. The identification results for both the L-LPV and the F-LPV model are shown in Fig. 2. The functional dependencies used here are

$$\begin{aligned} \Theta^1(p^1, s) &= \alpha^1 + \beta^1 e^{\phi^1 s}, \\ \Theta^2(p^2, s) &= \alpha^2 + \beta^2 e^{\phi^2 s}, \\ \Theta^3(p^3, s) &= \alpha^3 + \beta^3 e^{\phi^3 s}, \end{aligned} \tag{13}$$

where $p = \{\alpha,\ \beta,\ \phi\}$ is the set of parameters for each function, and where β^1 is negative and β^2 and β^3 are positive. Fig. 2 shows that the L-LPV model may have an advantage in terms of modelling accuracy, especially for θ^1. However, as the variance of the local models increases with the increasing sampling time and number of intervals, the F-LPV model has an advantage as it considers all local models and is thus able to filter out the (locally) poor models.

B. Model performance

Once all the models have been identified, we first evaluated their voltage prediction performance on the identification data set. From this we concluded that L-LPV and consequently F-LPV require a sufficient number of intervals, i.e., $I > 10$, to produce satisfying results. Furthermore, at low sampling times L-LPV outperforms F-LPV due to its ability

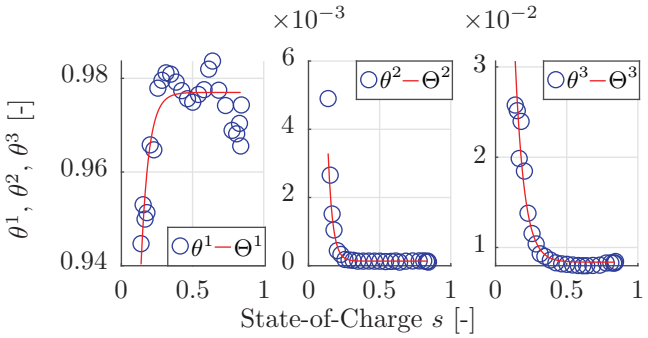

Fig. 2: Example of L-LPV (θ) and F-LPV (Θ) models at $T_s = T_m = 1s$ and $I = 25$.

to capture more detailed dependencies as depicted in Fig. 2. The performance of both L-LPV and F-LPV decreases as the sampling time increases. F-LPV remains more accurate, due to its ability to filter out poor local models, as explained in the previous section. For each sampling time, we now select the model with the number of intervals I corresponding to the lowest RMSE, and we plot them together with those of the LTI models, in Fig. 3a. This confirms that the error of L-LPV rises with the increasing sampling time, while that of F-LPV is relatively constant.

To validate prediction performance, we have tested the models on four different dynamic cycles and have calculated the RMSE for each of these cycles, which we have subsequently averaged to come to an average RMSE. The important features of these cycles, including the identification cycle, are provided in Table I. The same models used in Fig. 3a have now been applied to the validation cycles and the average RMSEs are shown in Fig. 3b. First of all, the errors for the LTI model are lower for the validation data than for the identification data. The LTI models have been fitted such that they represent the relatively constant dynamics at high SoC, i.e., above 25% SoC as also observed for the LPV models in Fig. 2. Since validation cycles two and four end at relatively high SoC, it is also expected that the LTI models perform better since the SoC dependency is minor in this SoC region, hence, have a lower RMSE. In terms of errors for L-LPV and F-LPV, we get comparable results for the identification and validation data, both confirming that F-LPV outperforms L-LPV at high sampling times.

TABLE I: Data features

	identification	validation* 1	* 2	* 3	* 4
time (h)	1.4	4.0	3.3	3.3	1.7
max SoC	0.85	0.97	0.97	0.85	0.95
min SoC	0.13	0.16	0.28	0.14	0.23

C. Current measurement sampling rate

Finally, let us consider the case in which all available current measurements, i.e., at each T_m, can be used when $T_s > T_m$. In (1), we see that the dynamics of the SoC are a perfect integrator and the overpotential state is an integrator with fading memory, because $\theta^1 < 1$. This suggests that there is an obvious benefit to using all available current

Authorized licensed use limited to: Technische Hochschule Deggendorf. Downloaded on September 13,2024 at 20:15:36 UTC from IEEE Xplore. Restrictions apply.

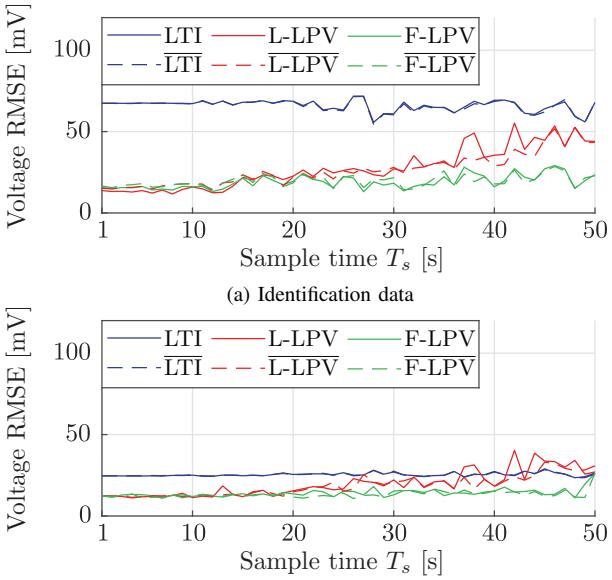

(a) Identification data

(b) Validation data

Fig. 3: RMSE of best models for each sampling time (continuous lines) and RMSE of best models with averaged current input for the state (dashed lines).

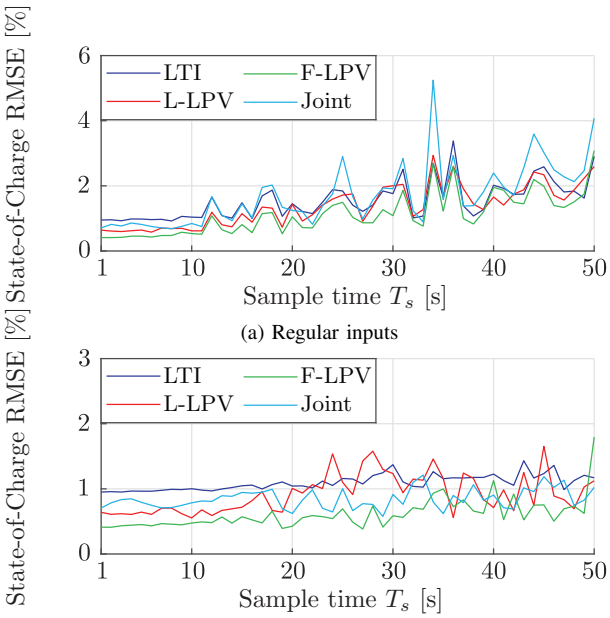

(a) Regular inputs

(b) Averaged state-input

Fig. 4: RMSE of SoC estimations for all four interpretations of the EKF, for both regular, as in (1), and for averaged state-inputs, as in (14).

measurements. Therefore, at time k we can also use the average of the past T_m input samples, given by

$$\overline{u}_k = \tfrac{1}{M} \sum_{\ell=0}^{M-1} u(kT_s - \ell T_m), \tag{14}$$

with $M = T_s$, as input for the state equation of (1), but keep using u_k for the output equation, because of the large impact that the voltage drop has on the terminal voltage. In the rest of this paper, we will refer to the inputs as in (1) as *regular* inputs and state inputs as in (14) as *averaged* inputs, where, as stated before, we consistently choose $T_m = 1s$ which allows us to capitalise on all available measurements. The effect of using this averaged input on the prediction performance is shown in the results in Fig. 3, where the dashed lines on average show a minor decrease in RMSE, especially at higher sampling times. This small difference is not surprising as we assume that the SoC is known in the results above. Consequently using (14) only impacts the accuracy of the overpotential state. In the next section, however, we will consider SoC estimation via the EKF. This heavily relies on current integration in the state equation, and thus the use of (14) is expected to have a significant impact on the performance.

V. SoC Estimation Results

In the previous section, we have determined the best model for each sampling time and we will now use these to estimate the SoC of the four validation cycles. After this, we will also execute the prediction and update steps of the EKF at different frequencies, where we will consider the trade-off between computation time and SoC estimation accuracy.

A. SoC estimation for varying sampling time

With the same models used for the results in Fig. 3, we have estimated the SoC of the four validation cycles. Each validation cycle contains two measurements of the current, one accurate measurement obtained with a lab-grade sensor (LEM IT 60-S ULTRASTAB) and one with a production-grade sensor (LEM DHAB S/133), typically used for automotive applications. In this case, the signal of the lab-grade sensor is used to determine the SoC reference and the one of the production-grade sensor, which is noisy and slightly biased, as input for the EKF.

The SoC estimation results are shown in Fig. 4, where the use of the regular current input, as in (1), shows an consistently decreasing SoC estimation accuracy until the sampling time $T_s > 11s$. Beyond this sampling time, the current inputs taken at the sampling instant possibly do not represent the average inputs over the preceding sampling period, which results in erratic performance. The benefit of using the average of the current measurements for the state equation is clear in Fig. 4b, as the RMSEs are more robust with respect to larger sampling times. Similar to the voltage prediction performance in Fig. 3b, the SoC estimation performance of LTI and L-LPV cross each other at large sampling times. The JEKF and F-LPV are similarly affected by the sampling time in the sense that they are relatively steady at first and become more erratic at higher sampling times.

B. EKF update frequency adjustment

Apart from changing the sampling time of the model, we can also alter the frequency with which the update step of the EKF is evaluated. For instance, after each passing of the sampling time, we evaluate the prediction step, as given

Authorized licensed use limited to: Technische Hochschule Deggendorf. Downloaded on September 13,2024 at 20:15:36 UTC from IEEE Xplore. Restrictions apply.

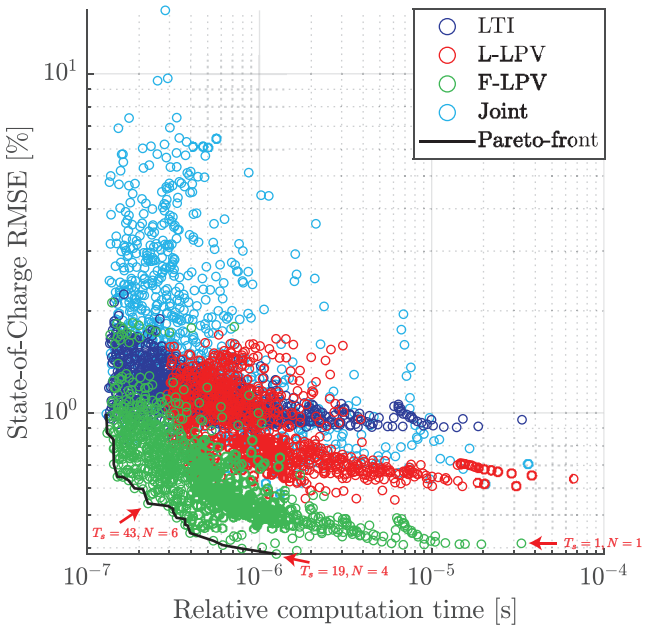

Fig. 5: Trade-off between relative computation time and SoC estimation error for all combinations of $T_s = \{1, 2, \ldots, 50\}s$ and $N = \{1, 2, \ldots, 20\}$, including Pareto-front.

by (8b) with $S = 0$, and once in every N passings of the sampling time we evaluate the entire EKF, where normally $N = 1$. In that sense the SoC estimation relies more on the current measurements and less on the voltage prediction for $N > 1$. To illustrate the effect of this, a series of $N = \{1, 2, \ldots, 20\}$ has been used to estimate the SoC of the four validation cycles, using the averaged state input of (14).

To see the effect of changing both the sampling time and update frequency with respect to estimation accuracy and the computational demand, let us consider Fig. 5. This shows the relative computation time per EKF evaluation, which is defined as the total computation time for one entire cycle divided by the number of seconds in that cycle, and is plotted against the RMSE of the SoC estimation. Note that both axes are logarithmic and the black line indicates the Pareto front. Comparing the most right green point (F-LPV, with $T_s = 1s$ and $N = 1$), with a number of similar SoC RMSE on the Pareto-front (F-LPV, with $T_s = 19s$ and $N = 4$), we observe a reduction in computational requirements of a factor 54. Allowing slightly larger RMSE, 0.54% for instance (F-LPV, with $T_s = 43s$ and $N = 6$), we obtain a reduction a factor 148. This means that SoC estimation of one cell can be done with the same computational load as those of 148 cells, while only increasing the estimation RMSE by 0.13%. As a result, SoC estimation for a full battery pack can be done with computational requirements comparable to estimating a few single cells at high frequency, thus enabling straightforward battery-pack SoC estimation.

VI. Conclusions

In this paper, the trade-off between SoC estimation performance and computation time using an Extended Kalman Filter (EKF) has been investigated by adjusting the update frequency and sampling time. We found that the combination of a higher sampling time and lower update frequency can still produce accurate SoC estimation results while significantly reducing the computational demand. One of the key factors was to use current measurements at a higher frequency than the sampling time of the model. Lowering the computational load of SoC estimation in this fashion, enables running an EKF per cell in a battery pack, instead of having to resort to sub-optimal approaches such as only estimating the SoC of a selection of cells. Therefore, this paper enables SoC estimation via the EKF to be applied to a large number of cells using limited computational resources and thus paves the way to straight-forward battery pack SoC estimation. Future work could study which system frequencies are dominant in batteries and which are excited by application-specific inputs. This can provide guidance in choosing an optimal sampling time for a specific application. Furthermore, different versions of the Kalman filter could be considered to see how they interact with applied overpotential models, which feature various degrees of nonlinearity.

References

[1] M. U. Cuma and T. Koroglu, "A comprehensive review on estimation strategies used in hybrid and battery electric vehicles," *Renewable and Sustainable Energy Reviews*, 2015.

[2] V. Pop, H. J. Bergveld, D. Danilov, P. P. L. Regtien, and P. Notten, *Battery Management Systems*. Springer, 2008.

[3] J. Hu, J. Hu, H. Lin, X. Li, C. Jiang, X. Qiu, and W. Li, "State-of-charge estimation for battery management system using optimized support vector machine for regression," *J. Power Sources*, 2014.

[4] G. L. Plett, "Extended Kalman filtering for battery management systems of LiPB-based HEV battery packs," *J. Power Sources*, 2004.

[5] M. Hannan, M. Lipu, A. Hussain, and A. Mohamed, "A review of lithium-ion battery state of charge estimation and management system in electric vehicle applications: Challenges and recommendations," *Renewable and Sustainable Energy Reviews*, 2017.

[6] Y. Wang, H. Fang, L. Zhou, and T. Wada, "Revisiting the State-of-Charge Estimation for Lithium-Ion Batteries: A Methodical Investigation of the Extended Kalman Filter Approach," *IEEE Control Systems Magazine*, 2017.

[7] J. Klee Barillas, J. Li, C. Günther, and M. A. Danzer, "A comparative study and validation of state estimation algorithms for Li-ion batteries in battery management systems," *Applied Energy*, 2015.

[8] J. Li, B. Greye, M. Buchholz, and M. A. Danzer, "Interval method for an efficient state of charge and capacity estimation of multicell batteries," *Journal of Energy Storage*, 2017.

[9] G. L. Plett, "Efficient Battery Pack State Estimation using Bar-Delta Filtering," in *Proc. EVS24*, 2009.

[10] Z. Zhang, X. Cheng, Z.-Y. Lu, and D.-J. Gu, "SOC Estimation of Lithium-Ion Battery Pack Considering Balancing Current," *IEEE Trans. Power Electron.*, 2018.

[11] H. Beelen, H. J. Bergveld, and M. C. F. Donkers, "Joint Estimation of Battery Parameters and State of Charge Using an Extended Kalman Filter: A Single-Parameter Tuning Approach," *IEEE Trans. Contr. Syst. Technol.*, 2020.

[12] R. Tóth, *Modeling and Identification of Linear Parameter-Varying Systems*. Springer, 2010.

[13] Y. Hu and S. Yurkovich, "Battery cell state-of-charge estimation using linear parameter varying system techniques," *J. Power Sources*, 2012.

[14] M. Einhorn, F. V. Conte, C. Kral, and J. Fleig, "Comparison, Selection, and Parameterization of Electrical Battery Models for Automotive Applications," *IEEE Trans. Power Electron.*, 2013.

[15] Y. Hu and S. Yurkovich, "Linear parameter varying battery model identification using subspace methods," *J. Power Sources*, 2011.

[16] B. Fridholm, M. Nilsson, and T. Wik, "Robustness comparison of battery state of charge observers for automotive applications," *IFAC Proceedings Volumes*, 2014.

Authorized licensed use limited to: Technische Hochschule Deggendorf. Downloaded on September 13,2024 at 20:15:36 UTC from IEEE Xplore. Restrictions apply.